Arab J Geosci (2016) 9: 482
DOI 10.1007/s12517-016-2512-9

ORIGINAL PAPER

A comprehensive VIKOR method for integration of various exploratory data in mineral potential mapping

Maysam Abedi[1] · **Reza Mohammadi**[1] · **Gholam-Hossain Norouzi**[1] · **Mir Saleh Mir Mohammadi**[1]

Received: 9 February 2016 / Accepted: 13 May 2016 / Published online: 26 May 2016

Abstract The central Iranian volcanic-sedimentary belt in Kerman province of Iran that is located within the Urumieh-Dokhtar magmatic arc zone is chosen to integrate diverse evidential layers for mineral potential mapping. The studied area has high potential of mineral occurrences especially porphyry copper, and the prepared potential maps aim to outline new prospect zones for further investigation. Two evidential layers including the downward continued map and the analytic signal of filtered magnetic data are generated to be used as geophysical plausible traces of porphyry copper occurrences. The low values of the resistivity layer acquired from airborne frequency domain electromagnetic data are also used as an electrical criterion in this study. Four remote sensing evidential layers including argillic, phyllic, propylitic, and hydroxyl alterations are extracted from Advanced Spaceborne Thermal Emission and Reflection Radiometer (ASTER) images in order to map the altered areas associated with porphyry copper deposits. The Enhanced Thematic Mapper Plus (ETM+) images are used as well to prepare iron oxide layer. Since potassic alteration is generally the mainstay of copper ore mineralization, the airborne potassium radiometry data is used to explore both phyllic and potassic alteration. Finally, the geochemical layers of Cu/B/Pb/Zn elements and the main geochemical component responsible for ore mineralization extracted from principal component analysis are included in the integration process to prepare final potential maps. The conventional and the extended version of VIKOR method (as a well-known algorithm in multi-criteria decision making problems) produced two mineral potential maps, and the results were compared with the ones acquired from prevalent methods of the index overlay and fuzzy logic operators of sum and gamma. The final mineral potential maps based upon desired geo-data set indicate adequately matching of high potential zones with previous working and active mines of copper deposits.

Keywords VIKOR method · Index overlay · Fuzzy logic operators · Mineral potential/prospectivity mapping · Porphyry copper deposit

✉ Maysam Abedi
MaysamAbedi@ut.ac.ir

[1] Department of Mining Engineering, College of Engineering, University of Tehran, Tehran, Iran

Introduction

Airborne geophysical survey is a prevalent effort in reconnaissance stage of various exploration projects that benefits predominant natural recourses industries such as mining, oil, and environment. These surveys as efficient tools in the primary stages of mineral exploration provide diverse pieces of information concerning the background geology of a deposit-type sought, as well as measure the geophysical variations arising from the different physical properties of the subsurface targets. They assist to cover large prospect areas simultaneously with multi-sensor geophysical equipment consisting of magnetic, radiometric, and electromagnetic devices. They subsequently cause lower cost in conducting such projects in a short time and provide advantageous information about geophysical characteristics of the desired sources. Therefore, these information can be used to mineral prospectivity modeling (MPM) (Abedi et al. 2015a).

MPM aims to detect new ore mineralization prospects and to delimit high potential zones of the mineralization in order to further explorations (Abedi and Norouzi 2016). Various exploration datasets (e.g., geological, geophysical, and

geochemical spatial data) must be collected, analyzed, and integrated for MPM. MPM process is a multi-criteria decision making (MCDM) operation that integrates numerous exploratory criteria/attributes and subsequently produces a predictive model to outline new prospective zones for further investigation (Yousefi and Carranza 2015a). Several MPM approaches are now reputable which can be categorized into two general groups of data- and knowledge-driven techniques (Pan and Harris 2000; Carranza 2008). Different evidential layers are extracted from the known deposit-type as training points (Bonham-Carter 1994) in order to establish linear or nonlinear spatial relationships between the known deposits and various layers of geological, geochemical, and geophysical criteria based upon numerous statistical/mathematical algorithms developed in data-driven groups (Carranza 2008). The sought relationships yield the importance and weight of each evidence layer (Carranza and Hale 2002a), and consequently, such layers are integrated into a single MPM by assigning the appropriate weights (Nykänen and Salmirinne 2007). The popular data-driven methods developed in the last two decades involve weights of evidence (e.g., Agterberg et al. 1990; Carranza and Hale 2002b), logistic regression (e.g., Agterberg and Bonham-Carter 1999; Carranza and Hale 2001; Mejía-Herrera et al. 2014), neural networks (e.g., Harris et al. 2003; Nykänen 2008; Abedi and Norouzi 2012), evidential belief functions (e.g., Carranza and Hale 2002c, 2003; Carranza et al. 2005, 2008a), Bayesian classifiers (e.g., Porwal et al. 2006; Abedi and Norouzi 2012), support vector machines (e.g., Zuo and Carranza 2011; Abedi et al. 2012a), clustering methods (Paasche and Eberle 2009; Eberle and Paasche 2012; Abedi et al. 2013a), and random forest method (e.g., Rodriguez-Galiano et al. 2014; Carranza and Laborte 2015). The other techniques in MPM process that were established based upon the geoscientist's opinions are known as the knowledge-driven approaches. They include the methods of Boolean logic approach (e.g., Bonham-Carter et al. 1989), index overlay (e.g., Carranza et al. 1999; Mirzaei et al. 2014; Sadeghi et al. 2014; Sadeghi and Khalajmasoumi 2015), Dempster–Shafer belief theory (e.g., Moon 1990; Carranza et al. 2008b), fuzzy logic operators (e.g., Abedi et al. 2013b; Moradi et al. 2015; Sadeghi and Khalajmasoumi 2015), wildcat mapping (e.g., Carranza and Hale 2002d), and different outranking methods (e.g., Abedi et al. 2015a; Abedi 2015b; Hossaini and Abedi 2015; Abedi et al. 2013c; Abedi et al. 2012b, 2012c; Pazand et al. 2012; Pazand and Hezarkhani 2015).

Nowadays, two new variants of MPM techniques are under development, compared to the conventional ones, namely (1) hybrid algorithm by simultaneous consideration of both location of known mineral occurrences and expert opinions (Porwal et al. 2003, 2004, 2006; Pazand and Hezarkhani 2015; Yousefi and Carranza 2015c) and (2) weighting to the continuous spatial evidence without using location of known mineral occurrences and without using expert judgments. Fuzzy logic MPM with continuous evidential data, data-driven index overlay, data-driven Boolean logic, expected value, and geometric average are the developed ones to overcome the bias resulting from (a) expert judgments in knowledge-driven MPM and from (b) using characteristics of known mineral occurrences in data-driven MPM (e.g., Yousefi and Carranza 2015b, 2016; Yousefi and Nykänen 2016).

Various MCDM algorithms have been developed to make an optimal decision in multi-criteria/attribute problems. Some of well-known ones were successfully accomplished in MPM (e.g., Abedi and Norouzi 2016; Abedi et al. 2015a; Abedi 2015). This study is the first attempt in MPM to evaluate the applicability of another MCDM algorithm, i.e., VIKOR technique proposed by Opricovic (1998), in data fusion of numerous evidential layers extracted from the airborne geophysical survey, satellite imagery, and geological and geochemical data sets in the desired area, pertaining to the central Iranian volcanic-sedimentary belt located in Kerman. Here, the efficiency of conventional and new formulation of the VIKOR algorithm (Opricovic and Tzeng 2004; Jahan et al. 2011) as a knowledge-driven method is figured out. We have revisited our previous exploratory geo-dataset comprising of 11 evidential layers (Abedi et al. 2015a) and have completed the database in this study by incorporating the information acquired from stream sediment geochemical data. The obtained results of the VIKOR method are compared to the outputs of the index overlay and the fuzzy logic operators algorithms, showing high matching of the generated MPMs. The validity of outputs were done by superimposing the location map of some active copper mines in the area, indicating good correlation between the copper mines and high potential zones of MPM maps.

The methodology, VIKOR algorithm in MPM

The VIKOR method was introduced by Opricovic (1998) as a powerful technique in MCDM problems to rank diverse attributes under different criteria or attributes. It determines the compromise solution and the weight stability intervals for preference stability of the compromise solution obtained with the initial assigned weights. The method is used to rank and select from a set of alternatives in the presence conflicting multi-criteria. It introduces the multi-criteria ranking index based upon the particular measure of "closeness" to the "ideal solution" (Opricovic 1998; Opricovic and Tzeng 2004). The following section describes concisely the formulation of the conventional and new version of VIKOR method.

Let us assume that $A_i (i = 1, 2, \ldots, n)$ and $C_j (j = 1, 2, \ldots, m)$ are a set of n alternatives and m criteria/attributes, respectively. The formulation of the conventional VIKOR method can be described in a series of steps;

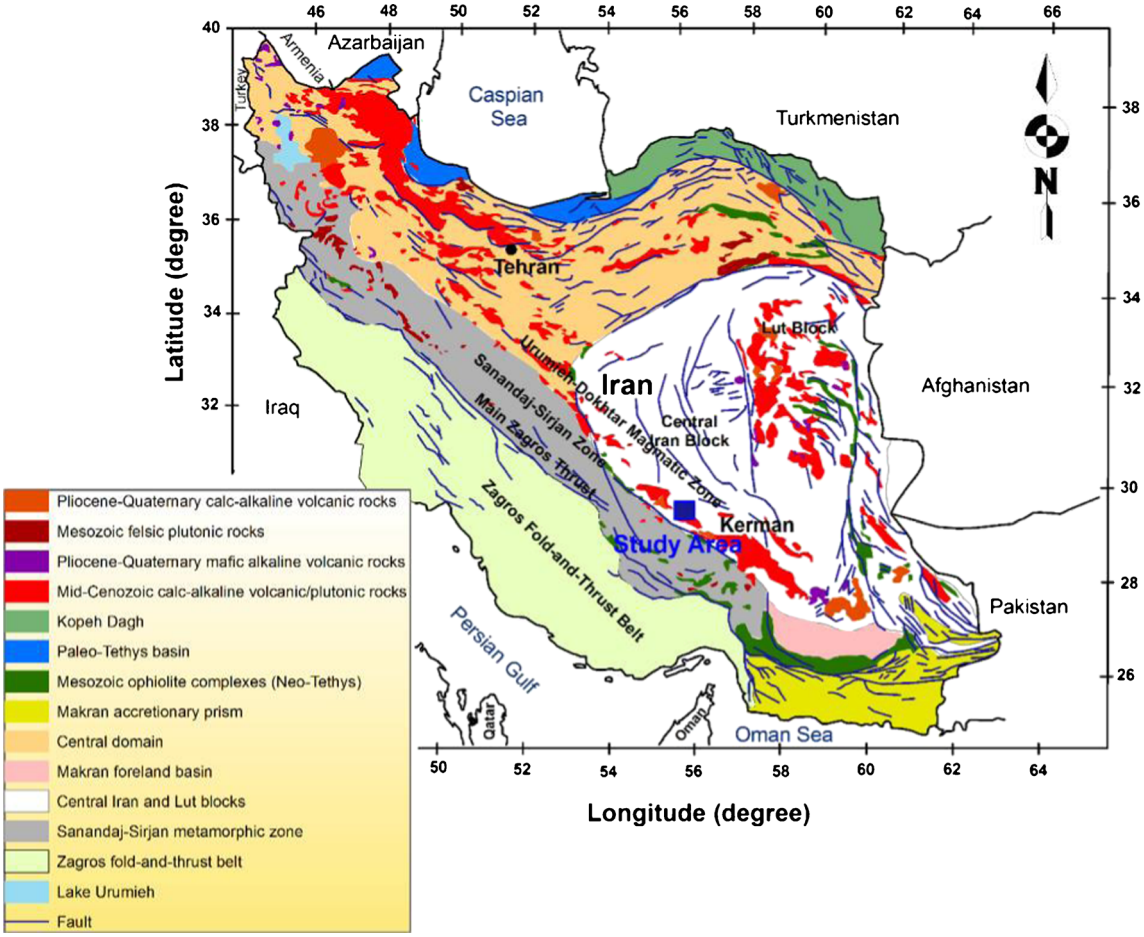

Fig. 1 Location of the studied area in the general geological map of Iran (reproduced from National Geoscience Database of Iran, http://www.ngdir.ir)

Stage 1. Construct a decision matrix acquired from a multi-disciplinary geo-dataset by assigning a priority score $X=(x_{ij})_{n\times m}$ to each alternative i on each criterion j.

Stage 2. Determine the important weight (w_j) of all criteria from developed methods (e.g., Delphi, AHP, Fuzzy-AHP techniques (e.g., Abedi et al. 2013b)) such that;

$$\sum_{j=1}^{m} w_j = 1, \quad j = 1, 2, \ldots, m. \tag{1}$$

Stage 3. Obtain the normalized decision matrix (r_{ij}). We should normalize each column of decision matrix to avoid scaling effects perturbing the VIKOR result.

$$r_{ij} = x_{ij} / \left(\sum_{p=1}^{n} x_{pj}^2 \right)^{0.5}, \quad i = 1, 2, \ldots, n \;\&\; j = 1, 2, \ldots, m \tag{2}$$

Stage 4. Determine the best f_j^+ and the worst f_j^- values of all criteria. If higher values of jth criterion are more favorable for ore occurrences (or benefit mode in MCDM problems), then

$$\begin{cases} f_j^+ = \max_i r_{ij} \\ f_j^- = \min_i r_{ij} \end{cases} \tag{3}$$

In cases that lower values of each criterion correspond to more favorable ore occurrences (or cost mode in MCDM problems), it is

$$\begin{cases} f_j^+ = \min_i r_{ij} \\ f_j^- = \max_i r_{ij} \end{cases} \tag{4}$$

Stage 5. Compute the values of S_i and R_i from the following equation. Development of the VIKOR method started from L_k metric as (Opricovic and Tzeng 2004),

$$L_{k,i} = \left(\sum_{j=1}^{m} \left[w_j \left(f_j^+ - r_{ij} \right) \Big/ \left(f_j^+ - f_j^- \right) \right]^k \right)^{1/k}, \quad 1 \le k \le \infty \tag{5}$$

Here, the values of S_i and R_i are calculated from the Eq. (5) to apply conventional VIKOR method:

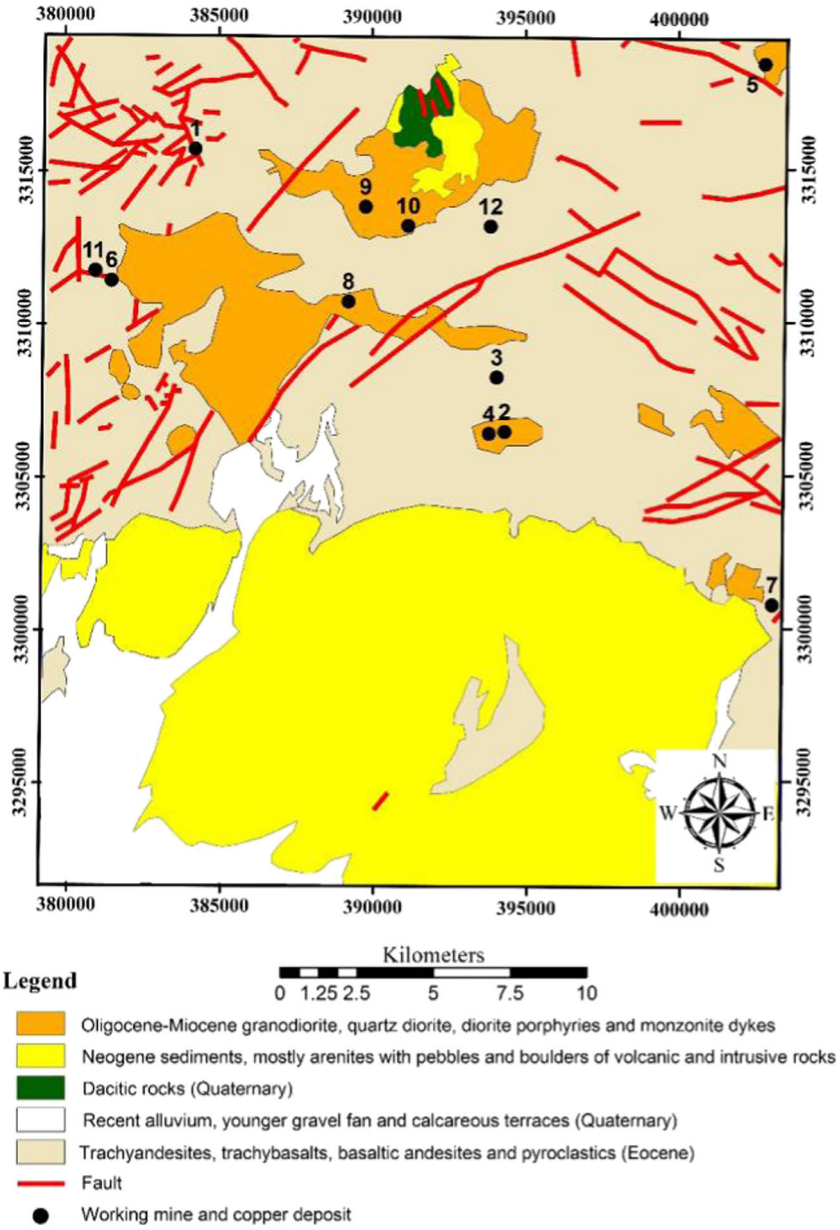

Fig. 2 Generalized 1:100,000 scale geological and mineral occurrence map of the study area located in Kerman province of Iran (reproduced from Ranjbar and Honarmand 2004; Abedi et al. 2013d)

$$S_i = L_{1,i} = \sum_{j=1}^{m} w_j \left(f_j^+ - r_{ij} \right) / \left(f_j^+ - f_j^- \right) \tag{6}$$

$$R_i = L_{\infty,i} = \max_j \left(w_j \left(f_j^+ - r_{ij} \right) / \left(f_j^+ - f_j^- \right) \right) \tag{7}$$

Stage 6. Compute the values of Q_i for each alternative i from the following equation:

$$Q_i = v\left(\frac{S_i - S^-}{S^+ - S^-}\right) + (1-v)\left(\frac{R_i - R^-}{R^+ - R^-}\right), \quad 0 \le v \le 1 \tag{8}$$

where

$$\begin{cases} S^+ = \max\limits_i S_i, S^- = \min\limits_i S_i \\ R^+ = \max\limits_i R_i, R^- = \min\limits_i R_i \end{cases}$$

and parameter v is introduced as a weight for the strategy of the majority of criteria "$\frac{S_i - S^-}{S^+ - S^-}$" and $(1-v)$ is the weight of the individual regret "$\frac{R_i - R^-}{R^+ - R^-}$." The value of v lies in the range of $[0, 1]$ and in most cases, it was chosen equal to $v = 0.5$ for a compromise solution (Jahan et al. 2011).

Stage 7. Compute MPM values of M_i for final prospectivity mapping as

Table 1 Main geological characteristics of all active mines in the study area (extracted from Ghorbani 2013)

ID	Name	Size	Host rock/age	Genetic/ mineralization	Orogenic phases	Morphology
1	Ardiz	Intermediate	Granite/Oligo-Miocene; rhyolite	Hydrothermal	Post-Pyrenean	Vein
2	Band-e-Mamezar1	Intermediate	Microdiorite/Oligo-Miocene; volcanics and pyroclastic/Eocene	Hydrothermal	Post-Pyrenean	Vein
3	Band-e-Mamezar2	Intermediate	Granodiorite/Oligo-Miocene; volcanics and pyroclastic/Eocene	Porphyry	Post-Pyrenean	Vein
4	DarrehZar	Large	Quartz microdiorite/Miocene; andesite, tuff/Eocene	Porphyry	Post-Pyrenean	Vein
5	Deh Siah Khan	Intermediate	Quartz monzonite and quartz diorite/Oligo-Miocene	Porphyry	Post-Pyrenean	Vein
6	Gowd-e-Konarak	Intermediate	Conglomerate, sandstone, and limestone/Miocene	Hydrothermal	Post-Pyrenean	Vein
7	Hoseyn Abad	Small	Porphyrite quartz diorite and diorite/Oligo-Miocene; andesite, dacite, pyroclastic, and sedimentary rocks/Late Eocene	Porphyry (?)	Post-Pyrenean	Vein
8	Nowchun	Large	Granite, porphyry diorite, and Rhyodacite/Oligo-Miocene; andesite and pyroclastic/Eocene	Hydrothermal	Post-Pyrenean	Vein
9	Piran	Small	Volcanics and pyroclastics/Eocene	Hydrothermal	Post-Pyrenean	Vein
10	Sar-Cheshmeh	Large	Granodiorite/Oligo-Miocene; andesite/Eocene	Porphyry	Post-Pyrenean	Vein
11	Sar-e-Kuh	Large	Granodiorite, porphyrite granodiorite, and porphyrite quartz diorite/Oligo-Miocene; volcano sedimentary rocks/Eocene	Porphyry	Post-Pyrenean	Vein
12	Seridun-e-Shomali	Intermediate	Andesite and dacite/Eocene	Hydrothermal	Post-Pyrenean	Vein, disseminated

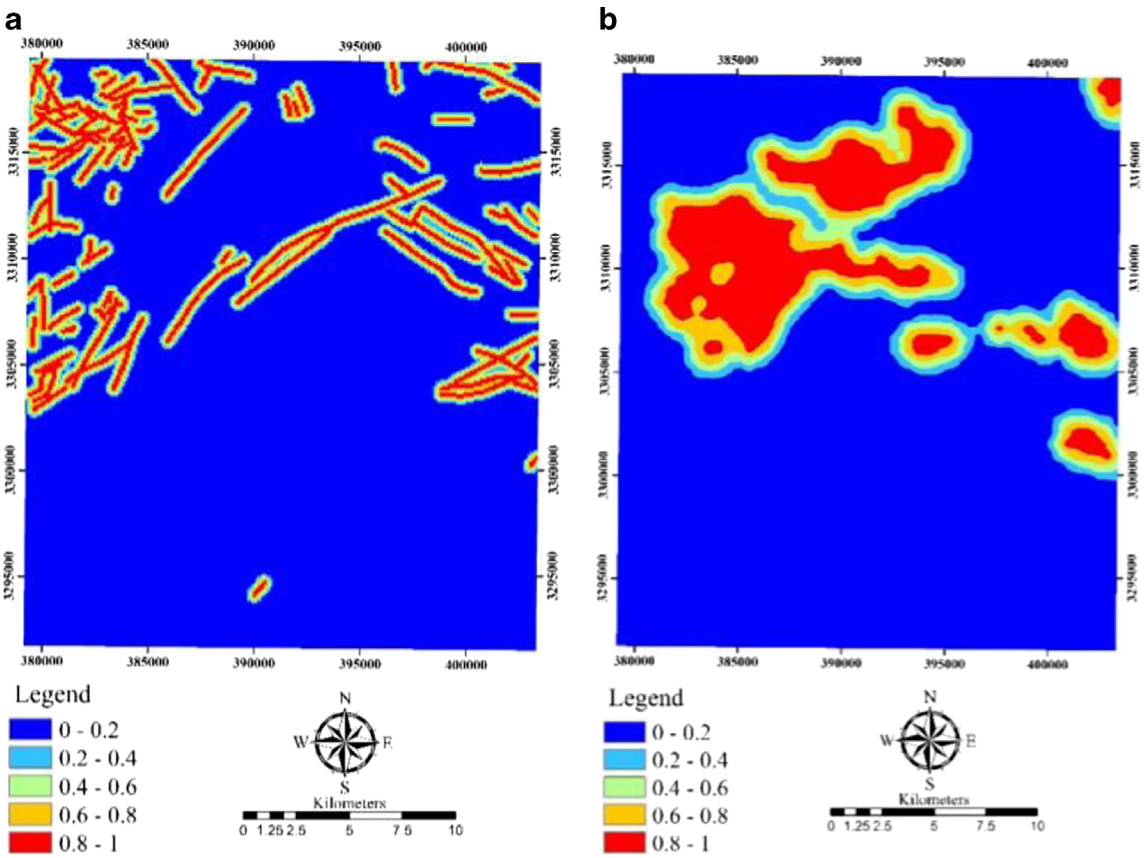

Fig. 3 Geological evidential layers: (**a**) faulted areas; (**b**) host rock zones. Higher values correspond to high potential zones in geological map

$$M_i = \frac{Q^+ - Q_i}{Q^+ - Q^-} \tag{9}$$

where $Q^+ = \max_i Q_i$ and $Q^- = \min_i Q_i$. Higher values of M_i correspond to higher potential zones for ore occurrences in the region of interest.

To implement new version of VIKOR method proposed by Jahan et al. (2011), the values of S_i and R_i are calculated from the following equations while the other steps are similar to the conventional VIKOR method.

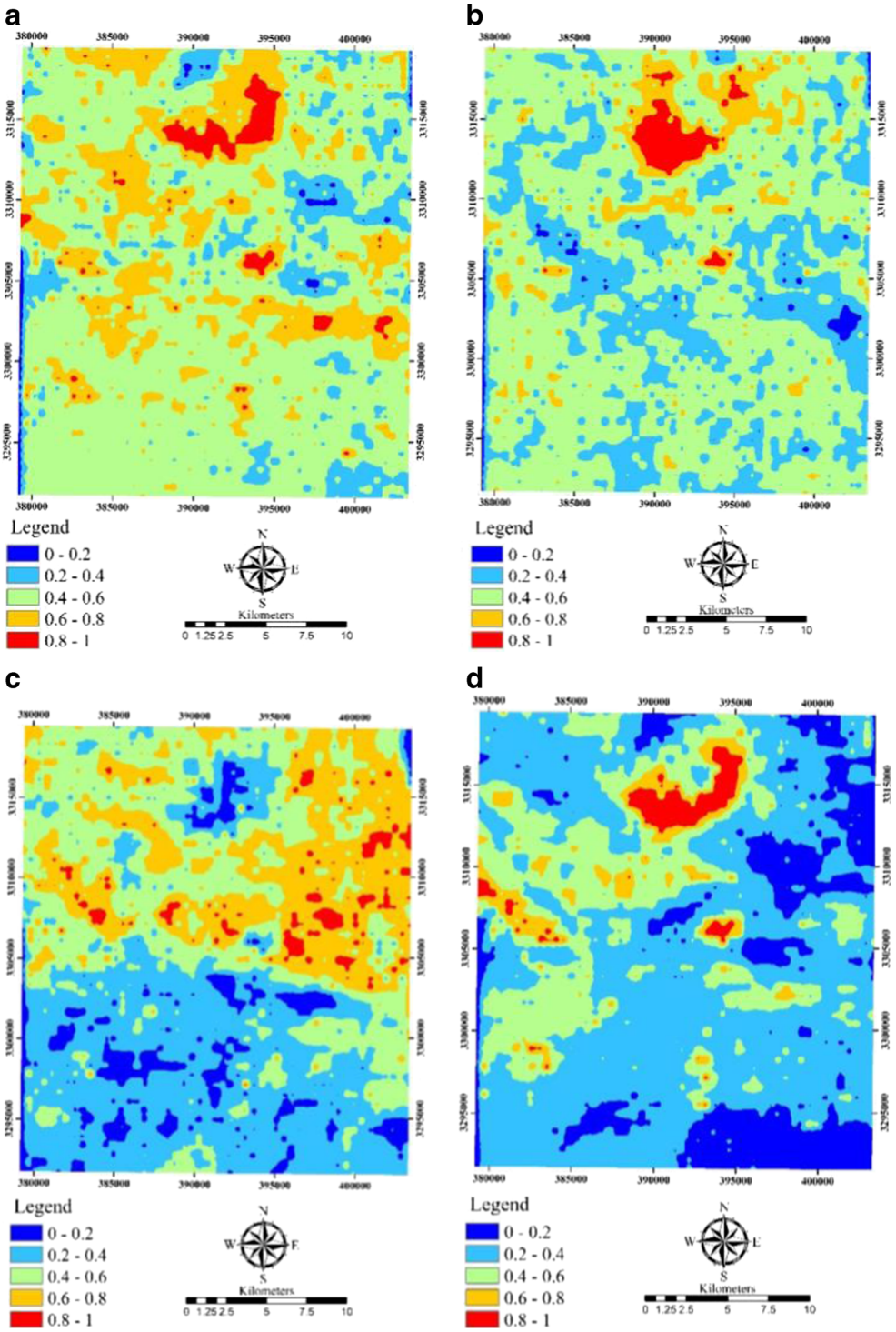

Fig. 4 Remote sensing evidential layers extracting alteration zones from ASTER data: (**a**) argillic; (**b**) phyllic; (**c**) propylitic; (**d**) hydroxyl

$$S_i = \sum_{j=1}^{m} w_j \left(1 - e^{\frac{|r_{ij} - f_j^+|}{f_j^- - f_j^+}}\right) \quad (10)$$

$$R_i = \max_j \left[w_j \left(1 - e^{\frac{|r_{ij} - f_j^+|}{f_j^- - f_j^+}}\right) \right] \quad (11)$$

Background geology

The prospect area is located within the Urumieh-Dokhtar Magmatic Assemblage (UDMA) arc of the Central Iran domain, where extensive Tertiary to Plio-Quaternary extrusive and intrusive units are exposed along a NW-SE trend (shown in Fig. 1). The output of various studies in this region state that a subduction-related magmatic model for the UDMA zone can be assumed (e.g., Alavi 1994; Berberian and Berberian 1981; Ahmad and Posht Kuhi 1993; Hassanzadeh 1993; Moradian 1997; Omrani et al. 2008) owing to the closure of the Neo-Tethyan ocean between Arabian and Eurasia plates. The UDMA zone as an Andean-type volcanic magmatic arc consists of frequent porphyry-type deposits (especially Cu occurrences) associated with granitoids, plutonic bodies, and volcanic rocks. Generalized geological and mineral occurrence map of the prospect area located in Kerman province at SE of Iran is indicated in Fig. 2. Oligocene-Miocene granodiorite, quartz diorite, diorite porphyries, and monzonite dykes are predominant rock types of probable ore mineralization in this area. Sar Cheshmeh as a well-known world-class porphyry copper ore deposit has occurred in this region by locating within the southern part of the Central Iranian Volcanic-Sedimentary complex, southwest of Kerman City. The main reason of porphyry copper mineralization at Sar Cheshmeh is associated with a granodioritic stock intruded into a folded and faulted early tertiary volcanic-sedimentary series of andesite, tuffs, ignimbrites, and agglomerates. A widespread potassic alteration zone exists in the center that has imprints of phyllic alteration, and such alteration is surrounded by a weak biotite and phyllic zone. Propylitic zone surrounds the whole complex and extends away for few kilometers. Ore mineralization occurs in the potassic, biotite, and phyllic zones. Hydrothermal alterations of chlorite, sericite, epidote, carbonate, silica, tourmaline, and clay minerals are common in this ore deposit, but phyllic, argillic, and propylitic alterations are more prevalent in whole prospect area (Ranjbar and Honarmand 2004; Abedi et al. 2015a). Main geological

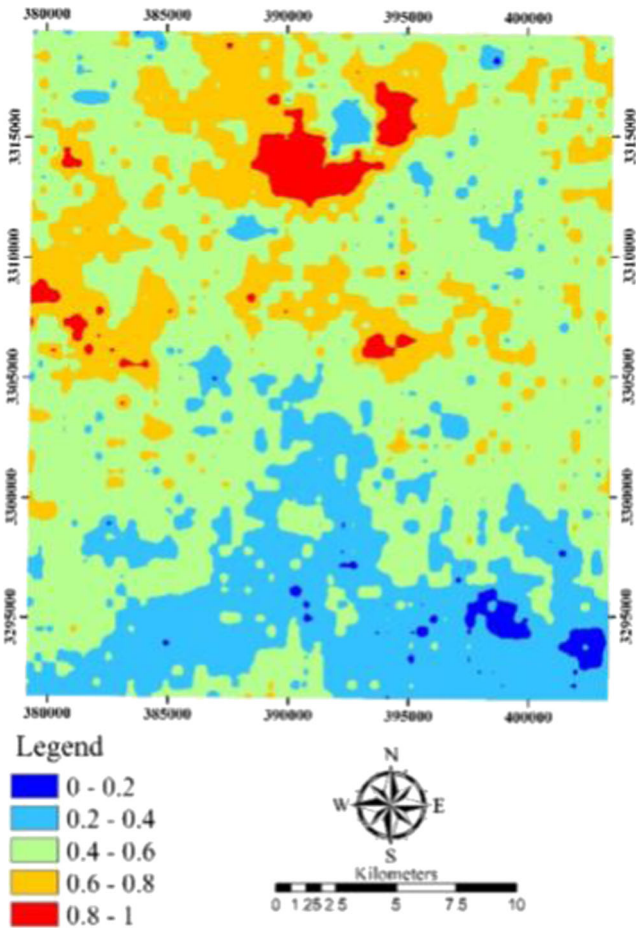

Fig. 5 Iron oxide alteration layer extracted from ETM+ bands

Table 2 The statistical summary of four elements were considered in final MPM

Statistics	Cu (ppm)	Pb (ppm)	Zn (ppm)	B (ppm)
Minimum	18	2	10	2
Maximum	1200	460	850	241
Range	1182	458	840	239
Mean	105.65	34.92	105.49	46.40
Median	71.00	24.00	94.00	39.00
Mode	68	2	72	7
Variance	18513.334	2229.429	4215.565	1067.633
Std. Deviation	136.064	47.217	64.927	32.675
Skewness	5.042	5.293	5.476	1.856
Kurtosis	30.608	35.181	50.054	5.860

Table 3 The linear correlation coefficient between five evidential geochemical layers

Cu	1				
Pb	0.654	1			
Zn	0.648	0.531	1		
B	0.697	0.510	0.504	1	
C_1	0.711	0.810	0.582	0.507	1
	Cu	Pb	Zn	B	C_1

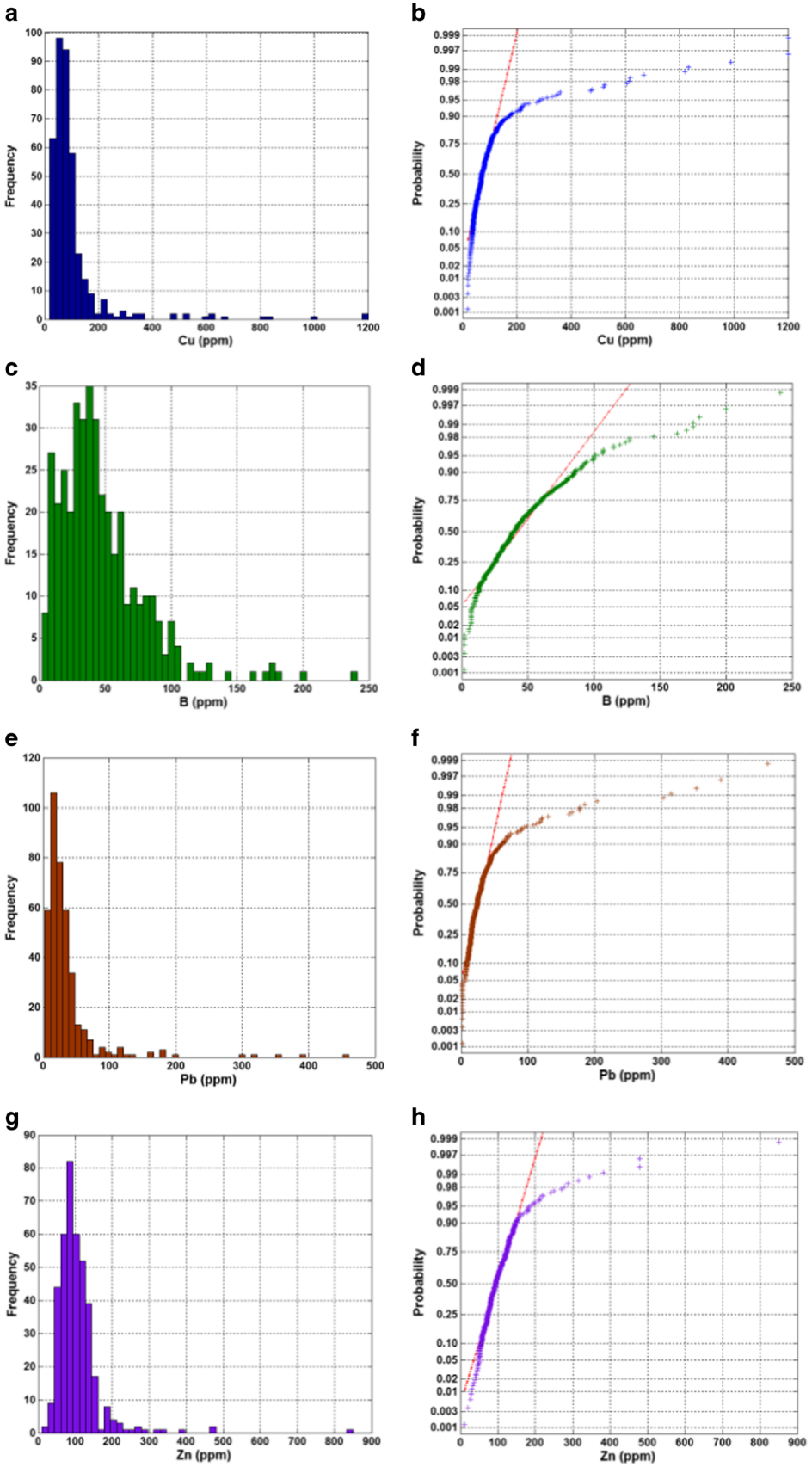

Fig. 6 Histogram and probability plots of four elements Cu, B, Pb, and Zn

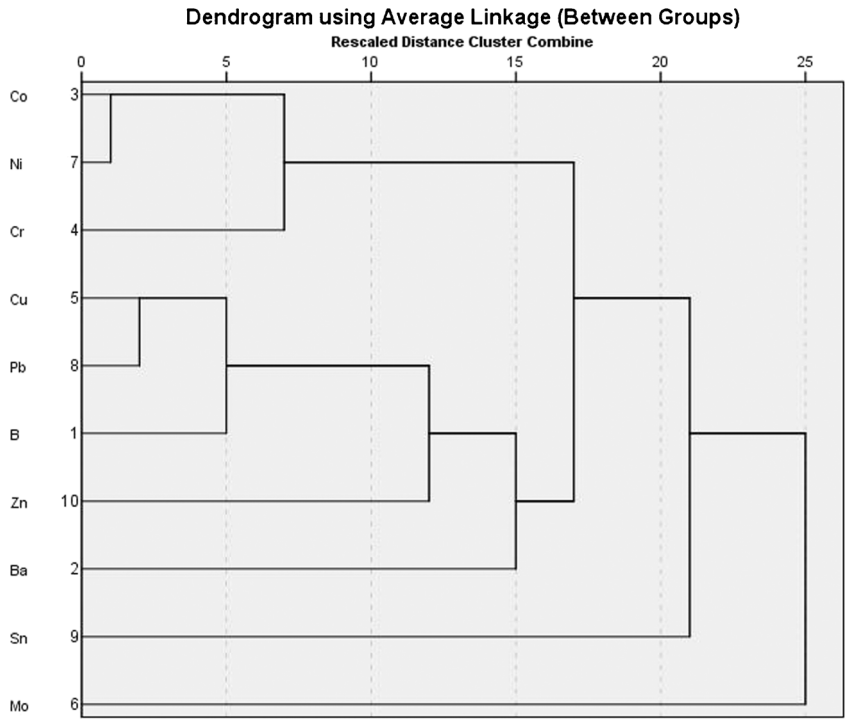

Fig. 7 Dendrogram of cluster analysis using average linkage method on stream sediment samples

characteristics of most active mines in the study area have been presented in Table 1.

Data setting

The following sub-sections discuss concisely all considered evidential layers extracted from geological map, satellite imagery data, stream sediment geochemical data, and airborne geophysics comprising of radiometric, magnetic, and Frequency Domain Electromagnetic (FDEM) data in order to generate mineral potential maps.

Geological layer

Two evidential layers of faulted areas and host rock zones were extracted by a group of geologists who are experts in MPM from the geological map shown in Fig. 2. These geological evidential maps show high potential zones which are more favorable for mineral occurrences (Fig. 3). According to the geology of the study area and the knowledge of decision making team, five 100-m-interval buffers are considered around fault lineation areas (Fig. 3a) to represent the faulted zones feature as a criterion in final preparation of MPM. Oligocene-Miocene granodiorite, quartz diorite, diorite porphyries, and monzonite dykes are the probable host rocks of the porphyry deposit in the studied area. Subsequently, four 250-m-interval buffers are considered in Fig. 3b around the mentioned units to represent the presence of mineralization (Abedi et al. 2015a).

Remote sensing layer

The alteration layers of argillic, phyllic, propylitic, hydroxyl, and iron oxide are common in most porphyry-type ore deposits. Here, band ratios of the Advanced Spaceborne Thermal Emission and Reflection Radiometer (ASTER) satellite imagery are used to extract these alterations in the study area. Because of the absence of an ASTER image in the blue region of the spectrum, iron oxide minerals cannot be enhanced from the ASTER data. Therefore, Enhanced Thematic Mapper Plus (ETM+) images are used to plot iron oxide alteration as well (Ranjbar et al. 2011; Gholami et al. 2012; Abedi et al. 2015a).

The study area has a semi-arid climate, a mountainous topography with a poor vegetation cover. Hence, it has great potential for exploration of porphyry-Cu deposits using remote sensing data (Abedi et al. 2015a). Mapping surface alterations using remote sensing sensors provides advantageous information in the reconnaissance stages of copper exploration especially at regional scales and arid areas. The shortwave length infrared (SWIR) spectral bands of ASTER images are a suitable tool for mapping hydrothermal alteration zones associated with porphyry-Cu deposits. Relative absorption band depth (RBD) was used by Abedi et al. (2013c, d; 2015a) to delineate

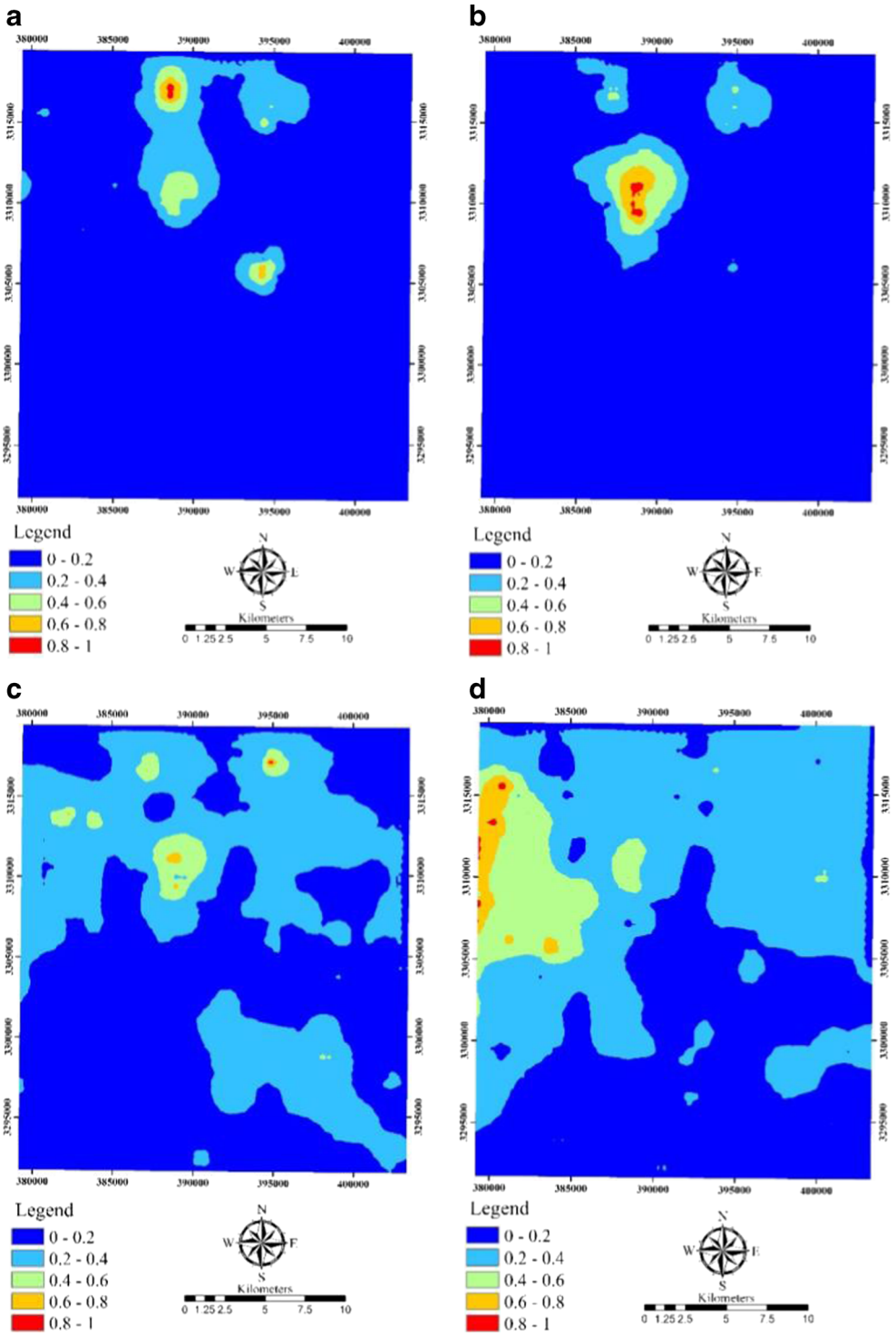

Fig. 8 Geochemical evidential layers with normalized values: (**a**) Cu, (**b**) Pb, (**c**) Zn, and (**d**) B

argillic, phyllic, propylitic, and hydroxyl mineral assemblages. Three RBD ratios adopted in this study namely RBD_5 (mineral features: alunite/kaolinite/pyrophyllite), RBD_6 (mineral features: sericite/muscovite/illite/

Table 4 PCA of stream sediment geochemical data for three main components. Component 1 was considered as a geochemical layer in final MPM

	Component		
	C_1	C_2	C_3
B	0.708	0.370	0.119
Ba	0.747	−0.142	0.018
Co	0.243	0.851	−0.060
Cr	0.039	0.775	0.171
Cu	0.750	0.421	−0.235
Mo	0.182	0.152	−0.775
Ni	0.104	0.828	−0.086
Pb	0.845	0.168	−0.007
Sn	0.228	0.246	0.696
Zn	0.450	0.468	0.168
% of variance	~40	~15	~12

smectite), and RBD_8 (mineral features: carbonate/chlorite/epidote) were used to delineate argillic, phyllic, and propylitic hydrothermal alteration zones (van der Meer et al. 2012). The RBD ratios have been derived based on Crowley et al. (1989) as follows:

$$RBD_5 = \frac{band4 + band6}{band5} \quad (12)$$

$$RBD_6 = \frac{band5 + band7}{band6} \quad (13)$$

$$RBD_8 = \frac{band7 + band9}{band8} \quad (14)$$

A band ratio corresponding to band4/(band6+band9) was used as well to map hydroxyl-bearing minerals (Abedi et al. 2013d). All alterations are shown respectively in Fig. 4a–d.

Since iron oxide minerals (e.g., goethite, hematite, and jarosite) by processing of ETM+ images are better localized and have higher resolution, the principal component analysis (PCA) as a multivariate statistical technique is applied to image such alteration shown in Fig. 5. Bands 1, 2, 3, and 4 of ETM+ images are in the visible and near infrared (VNIR) region, and bands 5 and 7 are in the SWIR region as well. Six ETM+ bands as input (bands 1, 2, 3, 4, 5, and 7) were incorporated in the PCA method to generate iron oxide altered areas (Abedi et al. 2013d).

Geochemical layer

To acquire geochemical information in the prospect area, 392 stream sediment samples were collected in a larger area (only 232 samples out of all locate in the studied area) and analyzed for 15 elements under the supervision of the Geological Survey of Iran (GSI). After statistically preparatory of all samples, it was found that three elements of Pb-Zn-B have more correlation with Cu concentration in the region. Table 2 has summarized the statistical characteristics of these elements, while their linear correlation coefficient with each other are presented in Table 3 showing high values respect to Cu element. The histogram and probability plots of these elements are shown in Fig. 6 indicating non-normal distribution of four geochemical elements. The average linkage algorithm based upon the average distance between cluster pairs was applied to 10 elements that have higher quality data in order to cluster

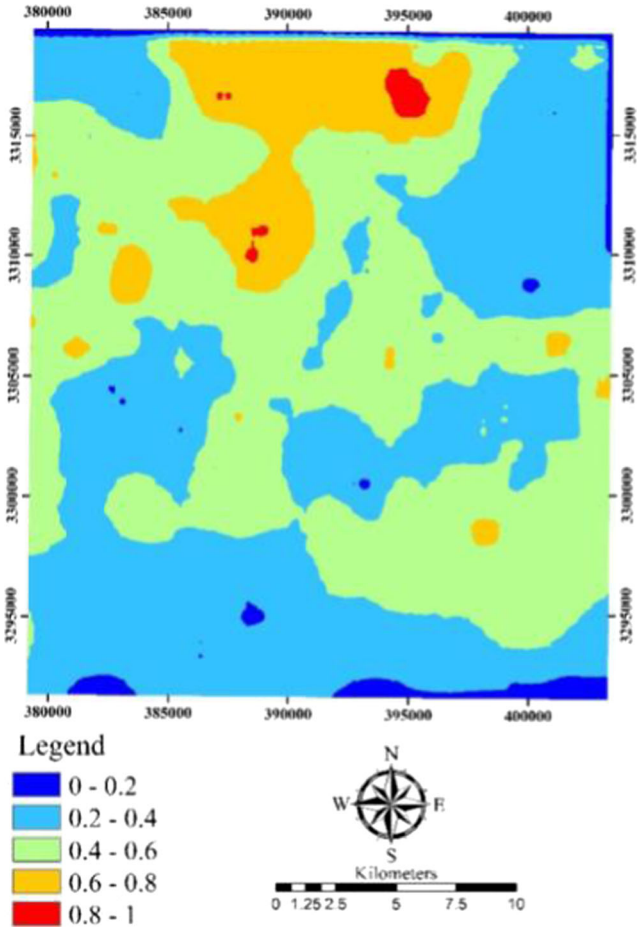

Fig. 9 Geochemical evidential layer extracted from the first component of PCA analysis

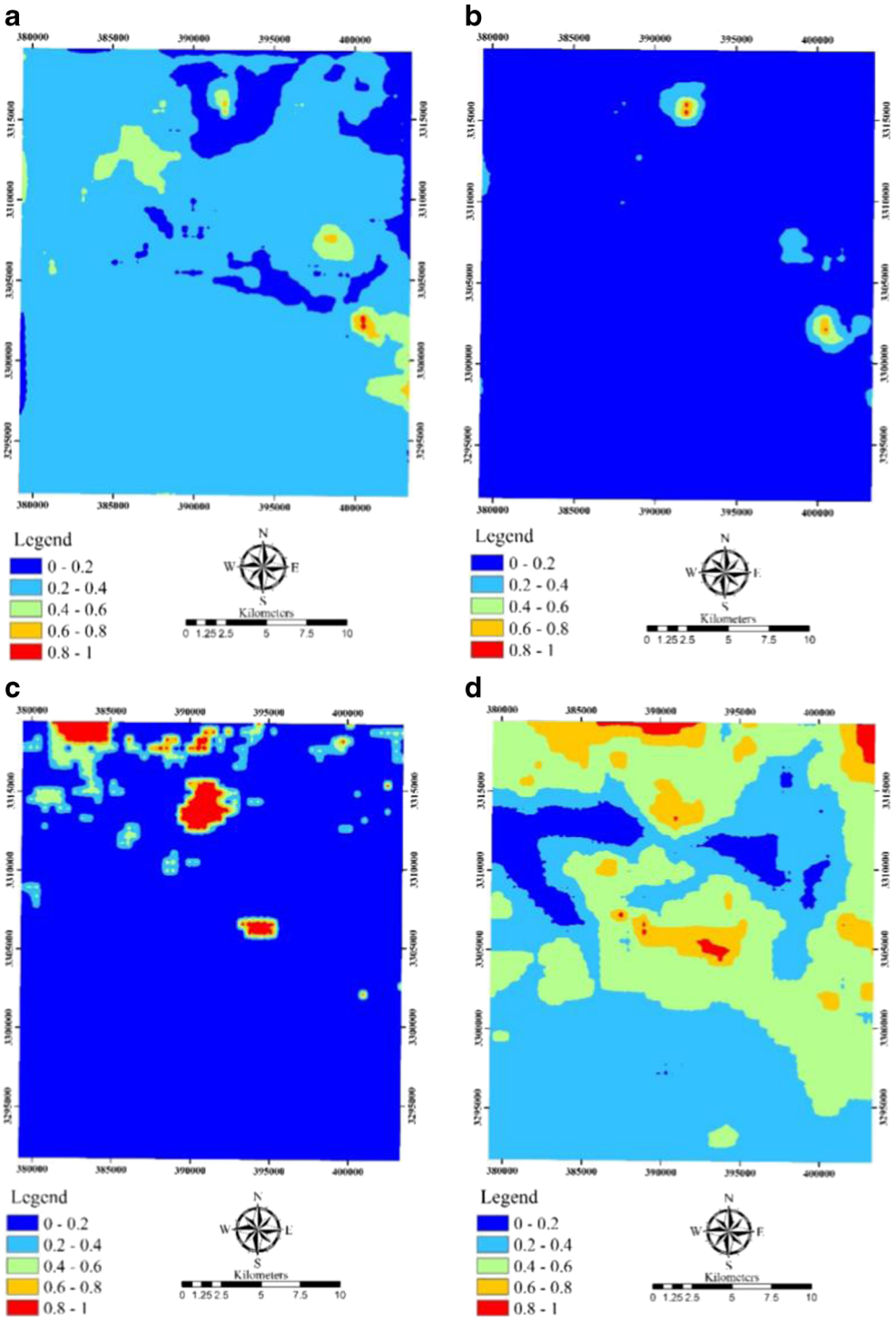

Fig. 10 Evidential geophysical layers: (**a**) downward continued magnetic data, (**b**) analytic signal of magnetic data, (**c**) resistivity, and (**d**) potassium radiometry. All layers were transformed to the interval of [0,1]

them in some groups. The variations within groups are low but between them are expected to be significant. The acquired dendrogram of clustering method is shown in Fig. 7, in which close similarity was observed between Cu/Pb/Zn and B. The geochemical layers of these elements shown in Fig. 8 were prepared to be incorporated in the final MPM map. All layers

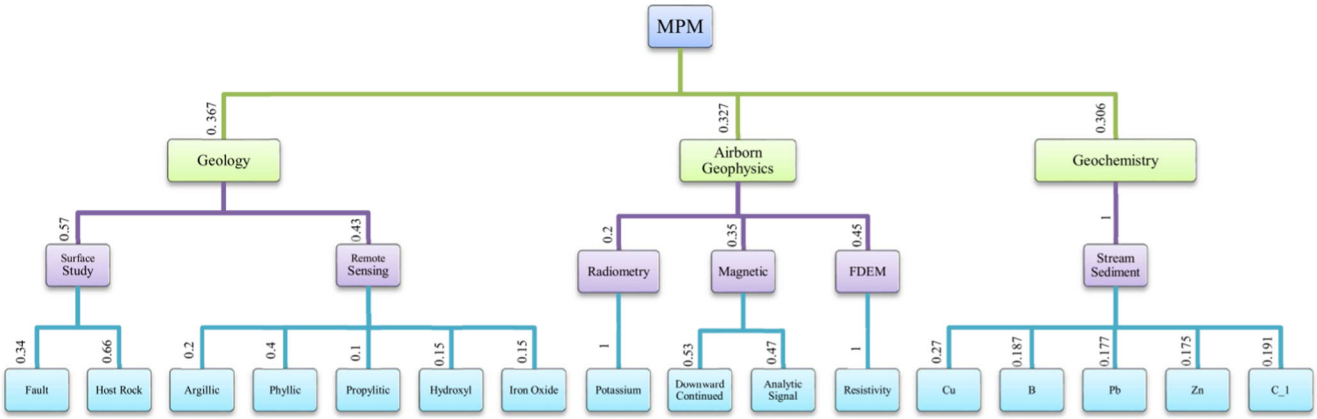

Fig. 11 Decision tree plot for preparation of final MPM. The weight of each evidential layer has been superimposed on the flowchart

have been plotted linearly at interval of [0,1] to not change the original distribution pattern of each element, in all which higher values correspond to more favorable mineral potential zones. It is worth mentioning that several algorithms have been developed to transform the geochemical data into a specific interval (Parsa et al. 2016a, b). Finally, the PCA algorithm was applied to 10 elements in order to extract main geochemical component related to Cu ore occurrences in the region. Table 4 presents three main components that show 67 % variance of all data. First component (C_1) corresponds to higher weights of four elements of Cu/Pb/Zn and B. This component shown in Fig. 9 could appropriately enhance the location of probable zones of copper occurrences in the region and was considered as another geochemical layer in MPM.

Geophysical layer

Alteration zones in porphyry-type deposits have a special magnetic signature that causes a specific pattern in magnetic maps. These magnetic patterns coincide with (1) increased concentration of secondary magnetite content in potassic/propylitic alteration zones, (2) magnetite

Table 5 The normalized weight of each criterion acquired from a group of geoscientist decision makers

Criterion	Weight	Sub-criterion	Weight	Sub-criterion	Weight	Final weight
Geology	0.367	Surface study	0.570	Fault	0.340	0.071
				Rock type	0.660	0.138
		Remote sensing	0.430	Argillic	0.200	0.032
				Phyllic	0.400	0.063
				Propylitic	0.100	0.016
				Hydroxyle	0.150	0.024
				Iron oxide	0.150	0.024
Geophysics	0.306	Radiometry	0.200	Potassium	1.000	0.061
		Magnetic	0.350	Downward	0.530	0.057
				Analytic signal	0.470	0.050
		FDEM	0.450	Resistivity	1.000	0.138
Geochemistry	0.327	Stream sediment	1.000	Cu	0.270	0.088
				B	0.187	0.061
				Pb	0.177	0.058
				Zn	0.175	0.058
				C_1	0.191	0.062

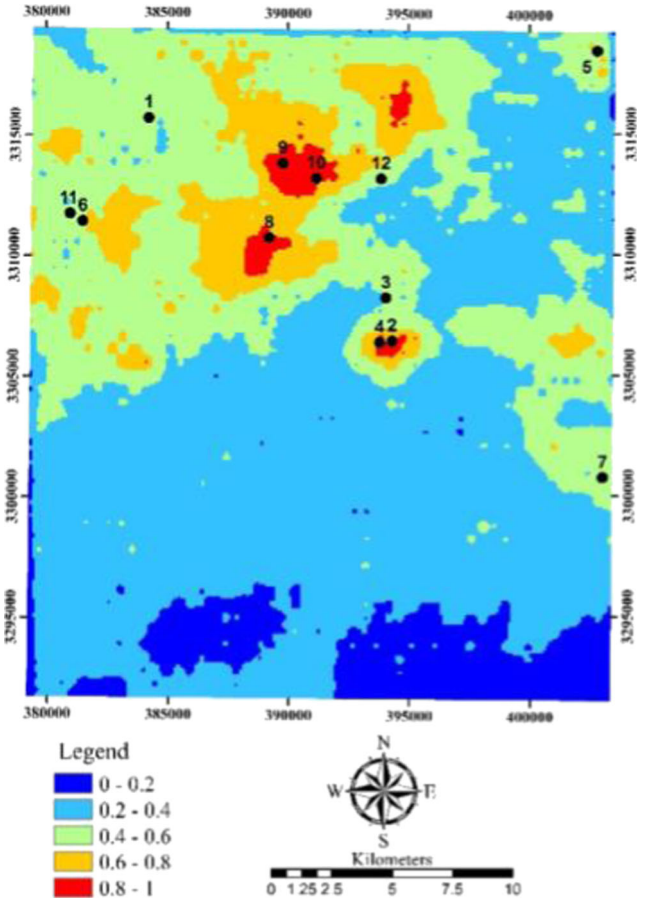

Fig. 12 The plot of index overlay (Io) MPM, on which the locations of active Cu mines have been superimposed

destruction in other lateral alterations, or (3) high magnetite in the main intrusive plutons responsible for mineralization (Daneshfar 1997; Pazand et al. 2012; Abedi et al. 2013d).

The airborne geophysical survey (magnetometry and potassium radiometry) was conducted in 1977 under supervision of the Atomic Energy Organization of Iran. Flight line spacing and height of survey were chosen 500 and 150 m, respectively. The collected data were in the form of a 1:50,000 scale geophysical contour maps and were converted into digital form by using on-screen digitization of contour lines. Thus, a set of 2601 data points were chosen to downward continued the reduced-to-pole (RTP) magnetic map at a height of 150 m to the ground surface in order to enhance subtle changes of earth's magnetic field arising from near surface causative sources. The main characteristic of the RTP technique is that it eliminates the dipolar nature of magnetic anomalies, converts their asymmetric shape to a symmetric shape, and put positive pole over the main source of anomaly. The 150-m stably downward continued map applied on the RTP data is shown in Fig. 10a (Abedi et al. 2013d).

Since the data integration of various evidential layers attempts to enhance probable near surface causative ore mineralization targets and as well these layers provide near surface exploratory information, the gradient of magnetic data aims to enhance such near surface effect. Therefore, the analytic signal method which was extensively discussed by Nabighian (1972, 1974, 1984) was applied to the downward continued data, in which high values of Fig.10b correspond to high potential zones of mineral occurrences (Abedi et al. 2013d). Since our case study is a part of a regional-scale prospect, high values of magnetic data were corresponded to high potential zones in order to enhance simultaneously potassic/ propylitic alterations and intrusive plutons responsible for Cu mineralization. These traces can play an important role in regional-scale Cu prospect to decrease the whole area of study into some potential zones (or deposit-scale zones). But in deposit-scale Cu prospect since the aim is to optimally locate boreholes location, the phyllic alteration is one of the main evidences of the Cu-bearing mineralization. Generally, this alteration is depleted of magnetite ore and subsequently reduces the magnetic susceptibility property of the main source of mineralization. Therefore, lower values of magnetic anomalies correspond to such alteration and recommended for exploratory borehole (Abedi et al. 2013e, 2015b).

FDEM data provide advantageous information about the electrical resistivity distribution for anomaly mapping in a variety of fields especially mineral exploration. The lateral resistivity variation can be displayed by apparent resistivity maps at single frequencies in FDEM survey (Siemon 2001). The line spacing of the conducted EM survey by Aerodat (a Canadian company) on behalf of the national Iranian copper industries company (NICICo) is 200 m, the sensor elevation was 30 m, and 5-frequency data acquisition system employed two vertical coaxial pairs at 912 and 4445 Hz, and three horizontal coplanar coil pairs at 516 Hz, 4131 Hz, and 32.37 KHz. Based upon the viewpoints of decision making team, the acquired apparent resistivity map at frequency 4445 Hz shown in Fig. 10c was processed to be included in the MPM.

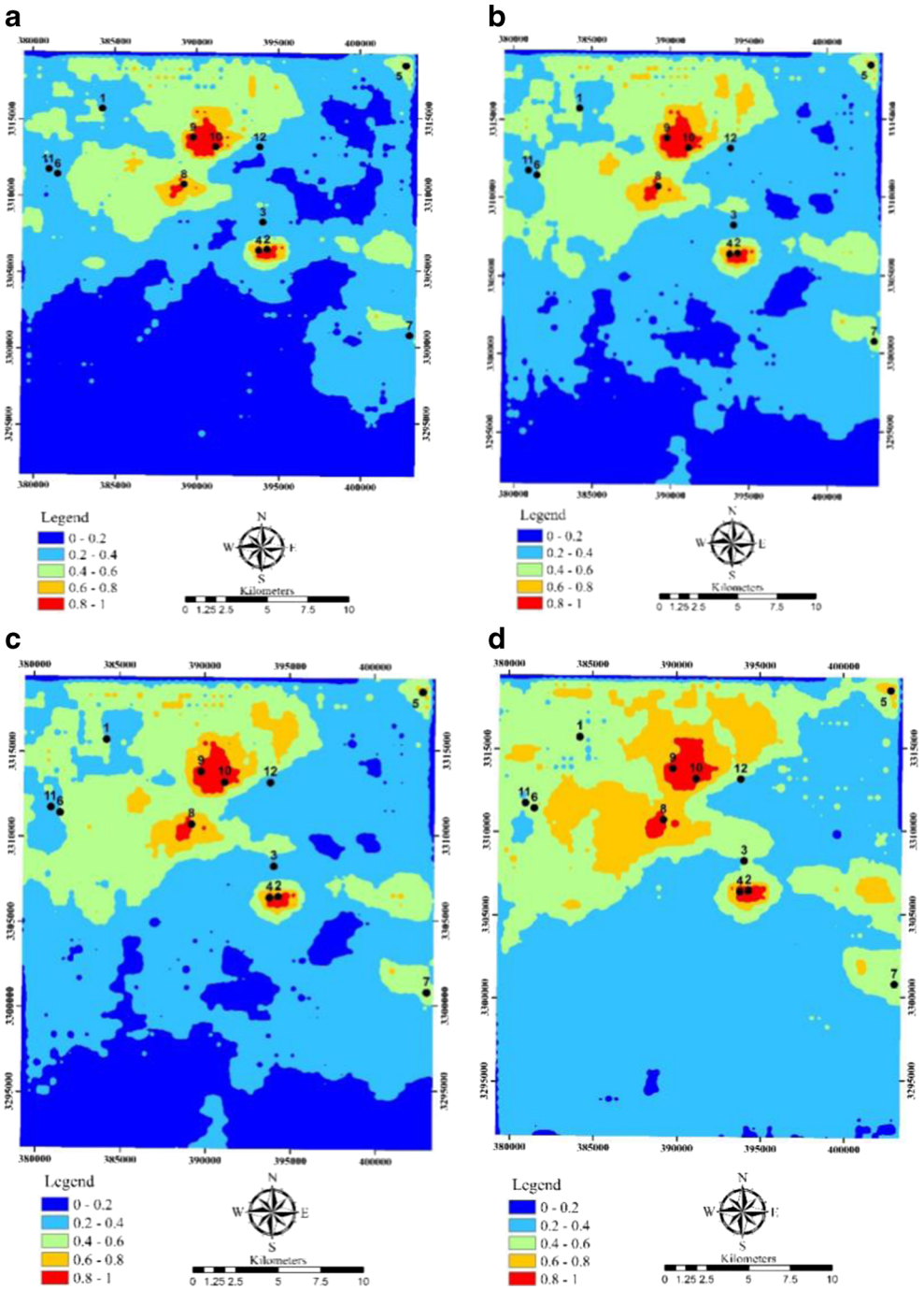

Fig. 13 The plot of fuzzy MPM, on which the locations of active Cu mines have been superimposed. Different gamma values of 0.8, 0.85, 0.90, and 0.95 were assumed to prepare MPMs of (**a**), (**b**), (**c**) and, (**d**) respectively

Hydrothermal alteration minerals (i.e., sericite, biotite, K-feldspars, and many K-bearing clay minerals) contain potassium (K) in porphyry-Cu deposits and are abundant particularly in the sericite zone. Therefore, K radiometric map shown in Fig. 10d can be used as a tool for exploration of such geological feature (Ranjbar and Honarmand 2004; Ranjbar et al. 2011; Abedi et al. 2013d). Chemical weathering also results in *K*

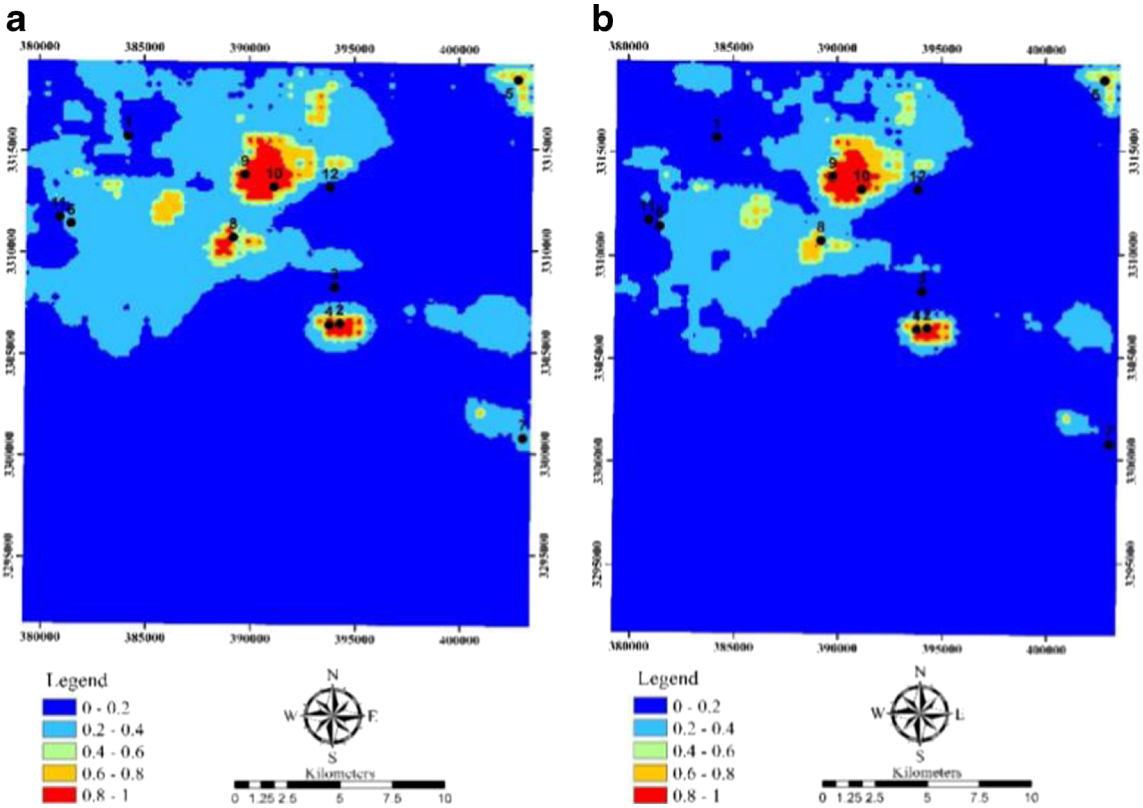

Fig. 14 The plot of VIKOR MPM: (**a**) the conventional approach and (**b**) the extended version on both the locations of active Cu mines have been superimposed

enrichment; therefore, it is preferable to use *Th*/*K* ratio. The *Th* radiometric map was not in access for decision makers to be used in this study.

Mineral potential mapping

To integrate sixteen prepared layers extracted from various geology, satellite imagery, airborne geophysics, and geochemical data, a decision matrix of $x_{2601 \times 16}$ was constructed in which 2601 alternatives and 16 evidential layers as criteria were considered. Each alternative corresponds to a location point with a specific coordinate in the study area. The decision tree map shown in Fig. 11 presents graphically the procedure of preparation final MPM. A group of geoscientists were gathered in a decision making team in order to assign the relative weigh of each criterion. These weights are tabulated in Table 5 such that $\sum_{j=1}^{16} w_j = 1$. Before applying the VIKOR method, the index overlay (Io) method as a linear combination of the weighted layers was applied to prepare final MPM. The output was plotted in Fig. 12 in which higher potential zones with more favorability for Cu occurrences correspond to higher values of the final MPM.

Another powerful algorithm for data fusion of various exploratory geo-dataset is the application of fuzzy operators in MPM (Abedi et al. 2013a). Here, fuzzy sum operator was used separately to integrate sub-criteria of each geology, airborne geophysics, and geochemical data. The produced fuzzy sum maps of these three criteria finally were integrated by fuzzy gamma (γ) operator. Four different values ($\gamma = 0.80, 0.85, 0.90, 0.95$) were assigned to produce fuzzy maps of Fig. 13. Higher normalized values of MPM maps are in good agreement with the location of active copper mines in the area.

The conventional and the extended VIKOR methods were used to produce MPM shown in Fig. 14. Similar to previous generated MPM maps by the index overlay and the fuzzy methods, high potential zones of both VIKOR maps correspond to the location of twelve active and working mines in the region. To better present the procedure of application of the VIKOR method, an illustrative example for a decision matrix of $x_{10 \times 16}$ is put in Table 6. Two columns of the old and new VIKOR contain the calculated values of Q_i acquired from the Eq. 8. These values are normalized at interval of $[0, 1]$ by Eq. 9 and finally plotted based upon those specific coordinates of X (m) and Y (m).

Table 6 Illustrative example of applying VIKOR method in MPM for 16 criteria as evidential layers and 10 alternatives

Alternative			Criteria/sub-criteria																VIKOR MPM	
Num	*X* (m)	*Y* (m)	Fault	Rock	Arg.	Phy.	Pro.	Hyd.	Iron	Pot.	DC.	AS.	Res.	Cu	B	Pb	Zn	C_1	Old V.	New V.
1	384136	3307755	0.009	0.800	0.221	0.538	0.997	0.245	0.664	0.182	0.380	0.067	0.009	0.105	0.512	0.085	0.212	0.459	0.15	0.16
2	398224	3317037	0.009	0.009	0.494	0.632	0.746	0.288	0.333	0.360	0.206	0.041	0.475	0.115	0.270	0.102	0.232	0.478	0.77	0.80
3	399199	3318137	0.009	0.009	0.238	0.553	0.742	0.054	0.617	0.411	0.191	0.022	0.500	0.078	0.269	0.066	0.160	0.435	0.85	0.88
4	389070	3318234	0.200	0.009	0.523	0.541	0.728	0.347	0.854	0.709	0.197	0.038	1.000	0.414	0.245	0.152	0.256	0.737	0.50	0.50
5	403405	3302584	0.009	0.009	0.554	0.372	0.721	0.393	0.410	0.700	0.399	0.180	0.710	0.053	0.161	0.028	0.173	0.435	0.72	0.74
6	380798	3311670	1.000	0.200	0.548	0.308	0.718	0.374	0.673	0.075	0.339	0.031	0.009	0.101	0.569	0.045	0.215	0.332	0.25	0.27
7	384602	3306088	0.600	0.600	0.408	0.268	0.715	0.465	0.405	0.309	0.219	0.087	0.009	0.088	0.525	0.066	0.161	0.374	0.22	0.26
8	402000	3307583	0.600	0.800	0.667	0.106	0.714	0.436	0.739	0.539	0.239	0.083	0.009	0.057	0.240	0.045	0.237	0.401	0.18	0.20
9	403535	3317544	0.800	0.600	0.000	0.008	0.000	0.000	0.705	0.896	0.077	0.059	0.009	0.001	0.001	0.005	0.001	0.001	0.47	0.44
10	395677	3302654	0.009	0.009	0.587	0.318	0.102	0.238	0.205	0.556	0.210	0.015	0.009	0.042	0.139	0.038	0.114	0.348	1.00	1.00

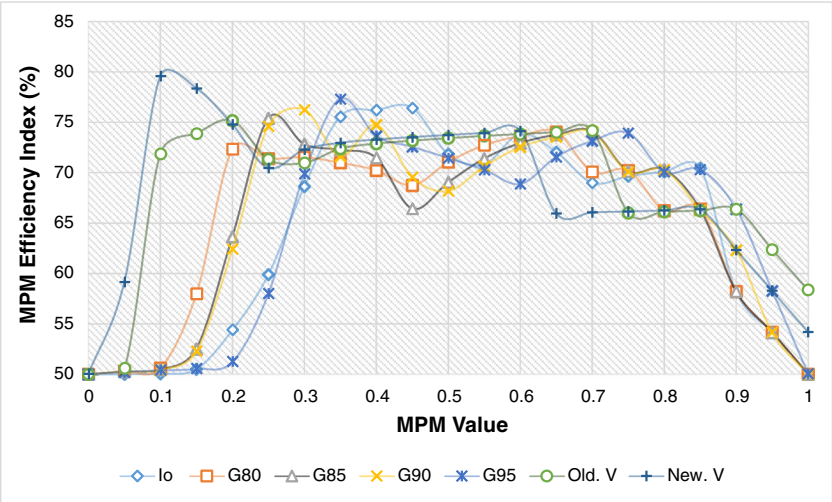

Fig. 15 The MPM efficiency index versus the MPM values for all applied algorithms of Index overlay (Io), Gamma values of 0.80, 0.85, 0.90, 0.95, and two new techniques of VIKOR, i.e., the conventional (old) and the extended (new) versions

To evaluate the performance of the applied methods in preparation of the final potential maps, the MPM efficiency index (MPM E.I.) is suggested to compare the produced maps. Such index is defined as:

$$\begin{aligned}\text{MPM Efficiency Index}\ (\%) \\ = w_1(100-\text{predicted area}\ \%) \\ + w_2(\text{ore prediction rate}\ \%)\end{aligned} \quad (15)$$

where $\sum_{i=1}^{2} w_i = 1$, and w_i shows the relative importance of each criterion. The prediction area corresponds to the ratio of the occupied area of prospectivity map to the whole study area. Ore prediction rate also corresponds to the percentage of known mineral occurrences predicted by the desired algorithm (or the ratio of the predicted deposit sources to the all deposit numbers in the studied region). Indeed, the MPM output is selected based upon such index that simultaneously predicts the highest numbers of the known deposit sources along with the lowest areas as potential zones. In cases that we chose $w_1 = w_2 = 0.5$ (the best unbiased weights), the MPM E.I. values are more than 50 %. Higher values of the index indicates that the produced MPM presents betted the prospectivity zones of mineral occurrences. Figure 15 shows the curve of this index versus the MPM values for all applied algorithms, considering an equal weight of 0.5 for each criterion. The extended version of VIKOR method produced the highest index equal to ~80 %. The average and maximum values of this index for all applied methods have been plotted in Fig. 16, showing that the proposed approach have higher values compared to the conventional methods. The information of twelve active Cu mines summarized in Table 1 have been used to calculate these index values.

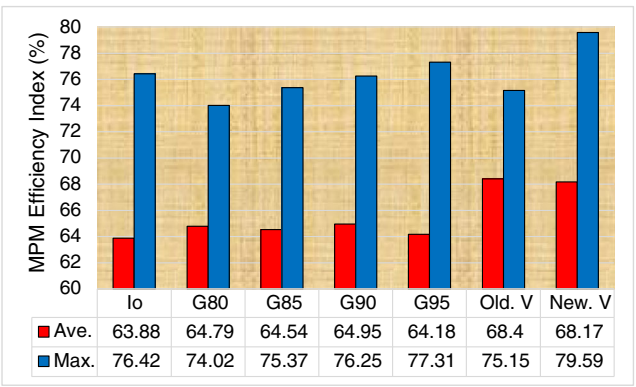

	Io	G80	G85	G90	G95	Old. V	New. V
Ave.	63.88	64.79	64.54	64.95	64.18	68.4	68.17
Max.	76.42	74.02	75.37	76.25	77.31	75.15	79.59

Fig. 16 The average and maximum values of the MPM efficiency index for all applied algorithms of Index overlay (Io), Gamma values of 0.80, 0.85, 0.90, 0.95, and two new techniques of VIKOR, i.e., the conventional (old) and the extended (new) versions

In this study, the data integration methods have been applied to the satellite imagery, the airborne geophysics, the sparse pattern of collected geochemical samples, and geological map with 1:100,000 scale. Therefore, the produced MPMs could only enhance high potential zones of Cu mineralization that should be considered for further investigations. In cases that ground-based geophysical data, field-based alteration mapping, denser collection of geochemical sample points, and using detailed geological map of the studied area (or collecting high frequency signals in the region) are used, it certainly yields the localization of high potential zones with higher resolution in mineral exploration. In this study, since we have used airborne data, low frequency data dominate the resulted MPM maps; therefore, some working mines like Hosen Abad could not be detected appropriately in the potential maps.

Conclusion

The presented work discussed for the first time the application of a well-known method in MCDM problems, i.e., the VIKOR technique, which could appropriately integrate various evidential layers extracted from a multi-disciplinary data sets pertaining to the central of Iran. The straightforward formulations of two variants of the method, i.e., the conventional and the extended versions, were explained in detail within the work. The MPM outputs of the proposed method were compared to the conventional methods of the index overlay and the fuzzy, while properly could enhance high potential zones responsible for copper occurrences in the region. The localized potential zones were also in good agreement with the locations of some active and working copper mines in the area. Furthermore, the MPM efficiency index as a tool of measuring performance of each applied method was proposed to evaluate the suitability of the MPMs. Such index considered simultaneously the predicted area and ore prediction rate as main factors in final decision of exploration program. It is worth to mention that the proposed approach could better present the prospectivity map of Cu occurrences in analogous with the conventional methods. As a consequence, the VIKOR method can be an effective approach in mineral potential mapping when various exploration criteria must be incorporated in datasets.

Acknowledgments The authors gratefully acknowledge the support provided by the Departments of Mining Engineering, University of Tehran. The Editor-in-Chief of the Arabian Journal of Geosciences, Prof. Al-Amri, and two respectful reviewers are also appreciated for their constructive and noteworthy comments which helped us to improve the quality and the presentation of the work.

References

Abedi M (2015) Reply to the comment by B. Ghobadipour and B. Mojarradi "M. Abedi, S.A. Torabi, G.-H. Norouzi and M. Hamzeh; ELECTRE III: A knowledge-driven method for integration of geophysical data with geological and geochemical data in mineral prospectivity mapping". J Appl Geophys 117:138–140

Abedi M, Norouzi GH (2012) Integration of various geophysical data with geological and geochemical data to determine additional drilling for copper exploration. J Appl Geophys 83:35–45

Abedi M, Norouzi GH (2016) A general framework of TOPSIS method for integration of airborne geophysics, satellite imagery, geochemical and geological data. Int J Appl Earth Obs Geoinf 46:31–44

Abedi M, Norouzi GH, Bahroudi A (2012a) Support vector machine for multi-classification of mineral prospectivity areas. Comput Geosci 46:272–283

Abedi M, Torabi SA, Norouzi GH, Hamzeh M, Elyasi GR (2012b) PROMETHEE II: a knowledge-driven method for copper exploration. Comput Geosci 46:255–263

Abedi M, Torabi SA, Norouzi GH, Hamzeh M (2012c) ELECTRE III: a knowledge-driven method for integration of geophysical data with geological and geochemical data in mineral prospectivity mapping. J Appl Geophys 87:9–18

Abedi M, Norouzi GH, Torabi SA (2013a) Clustering of mineral prospectivity area as an unsupervised classification approach to explore Copper Deposit. Arab J Geosci 6:3601–3613

Abedi M, Torabi SA, Norouzi GH (2013b) Application of fuzzy-AHP method to integrate geophysical data in a prospect scale, a case study: seridune copper deposit. Boll Geofis Teor Appl 54:145–164

Abedi M, Norouzi GH, Fathianpour N (2013c) Fuzzy Outranking Approach: a knowledge-driven method for mineral prospectivity mapping. Int J Appl Earth Obs Geoinf 21:556–567

Abedi M, Gholami A, Norouzi GH (2013d) A stable downward continuation of airborne magnetic data: a case study for mineral prospectivity mapping in Central Iran. Comput Geosci 52:269–280

Abedi M, Gholami A, Norouzi GH, Fathianpour N (2013e) Fast inversion of magnetic data using Lanczos bidiagonalization method. J Appl Geophys 90:126–137

Abedi M, Norouzi GH, Fathianpour N (2015a) Fuzzy ordered weighted averaging method: a knowledge-driven approach for mineral potential mapping. Geophys Prospect 63:461–477

Abedi M, Siahkoohi HR, Gholami A, Norouzi GH (2015b) 3D inversion of magnetic data through wavelet based regularization method. Int J Min Geol Eng 49:1–18

Agterberg FP, Bonham-Carter GF (1999) Logistic regression and weights of evidence modeling in mineral exploration. Proceedings of the 28th International Symposium on Applications of Computer in the Mineral Industry (APCOM), Golden, Colorado: pp. 483–490

Agterberg FP, Bonham-Carter GF, Wright DF (1990) Statistical pattern integration for mineral exploration. In: Gaál G, Merriam DF (eds) Computer applications in resource estimation. Pergamon Press, Oxford, pp 1–21

Ahmad T, Posht Kuhi M (1993) Geochemisty and petrogenesis of Urumiah–Dokhtar volcanics around Nain and Rafsanjan areas: a preliminary study. Treatise on the Geology of Iran, Iranian Ministry of Mines and Metals: 90 pp

Alavi M (1994) Tectonics of the Zagros orogenic belt of Iran: new data and interpretations. Tectonophysics 229:211–238

Berberian F, Berberian M (1981) Tectono-plutonic episodes in Iran. Geol Surv Iran Rep 52:566–593

Bonham-Carter GF (1994) Geographic information systems for geoscientists: modelling with GIS. Pergamon Press, Oxford, 398 pp

Bonham-Carter GF, Agterberg FP, Wright DF (1989) Weights-of-evidence modelling: a new approach to mapping mineral potential. In: Agterberg FP, Bonham-Carter GF (Eds.) Statistical Applications in the Earth Sciences. Paper, 89–9. Geological Survey of Canada, pp. 171–183

Carranza EJM (2008) Geochemical anomaly and mineral prospectivity mapping in GIS. Handbook of Exploration and Environmental Geochemistry, 11th edn. Elsevier, Amsterdam, p 351

Carranza EJM, Hale M (2001) Logistic regression for geologically constrained mapping of gold potential, Baguio district, Philippines. Explor Min Geol 10:165–175

Carranza EJM, Hale M (2002a) Spatial association of mineral occurrences and curvilinear geological features. Math Geol 34:203–221

Carranza EJM, Hale M (2002b) Where porphyry copper deposits are spatially localized? A case study in Benguet province, Philippines. Nat Resour Res 11:45–59

Carranza EJM, Hale M (2002c) Evidential belief functions for data-driven geologically constrained mapping of gold potential, Baguio district, Philippines. Ore Geol Rev 22:117–132

Carranza EJM, Hale M (2002d) Wildcat mapping of gold potential, Baguio district, Philippines. Trans Inst Min Metall (Appl Earth Sci) 111:100–105

Carranza EJM, Hale M (2003) Evidential belief functions for data-driven geologically constrained mapping of gold potential, Baguio district, Philippines. Ore Geol Rev 22:117–132

Carranza EJM, Laborte AG (2015) Random forest predictive modeling of mineral prospectivity with small number of prospects and data with missing values in Abra (Philippines). Comput Geosci 74:60–70

Carranza EJM, Mangaoang JC, Hale M (1999) Application of mineral exploration models and GIS to generate mineral potential maps as input for optimum land-use planning in the Philippines. Nat Resour Res 8:165–173

Carranza EJM, Woldai T, Chikambwe EM (2005) Application of data-driven evidential belief functions to prospectivity mapping for aquamarine-bearing pegmatites, Lundazi district, Zambia. Nat Resour Res 14:47–63

Carranza EJM, Wibowo H, Barritt SD, Sumintadireja P (2008a) Spatial data analysis and integration for regional-scale geothermal potential mapping, West Java, Indonesia. Geothermics 33:267–299

Carranza EJM, van Ruitenbeek FJA, Hecker CA, van der Meijde M, van der Meer FD (2008b) Knowledge-guided data-driven evidential belief modeling of mineral prospectivity in Cabo de Gata, SE Spain. Int J Appl Earth Obs Geoinf 10:374–387

Crowley JK, Brickey DW, Rowan LC (1989) Airborne imaging spectrometer data of the Ruby Mountains, Montana: mineral discrimination using relative absorption band-depth images. Remote Sens Environ 29:121–134

Daneshfar B (1997) An evaluation of indicators of prospectivity and potential mapping of porphyry deposits in middle and southern British Columbia by a GIS study of regional geochemical and other geoscientific data. Ph.D. thesis, University of Ottawa, Canada

Eberle DG, Paasche H (2012) Integrated data analysis for mineral exploration: a case study of clustering satellite imagery, airborne gamma-ray, and regional geochemical data suites. Geophysics 77:B167–B176

Gholami R, Moradzadeh A, Yousefi M (2012) Assessing the performance of independent component analysis in remote sensing data processing. J Indian Soc Remote Sens 40:577–588

Ghorbani M (2013) The economic geology of Iran, mineral deposits and natural resources. Springer, Dordrecht, 569 p

Harris DP, Zurcher L, Stanley M, Marlow J, Pan G (2003) A comparative analysis of favourability mappings by weights of evidence, probabilistic neural networks, discriminant analysis, and logistic regression. Nat Resour Res 12:241–255

Hassanzadeh J (1993) Metallogenic and tectonomagmatic events in the SE sector of the Cenozoic active continental margin of central Iran. University of California, Los Angeles, pp 1–204

Hossaini SA, Abedi M (2015) Data envelopment analysis: a knowledge-driven method for mineral prospectivity mapping. Comput Geosci 82:111–119

Jahan A, Mustapha F, Yousof Ismail M, Sapuan SM, Bahraminasab M (2011) A comprehensive VIKOR method for material selection. Mater Des 32:1215–1221. doi:10.1016/j.cageo.2015.06.006

Mejía-Herrera P, Royer JJ, Caumon G, Cheilletz A (2014) Curvature attribute from surface-restoration as predictor variable in Kupferschiefer copper potentials: an example from the Fore-Sudetic Region. Nat Resour Res. doi:10.1007/s11053-014-9247-7

Mirzaei M, Afzal P, Adib A, Khalajmasoumi M, Zarifi AZ (2014) Prospection of iron and manganese using index overlay and fuzzy logic methods in balvard 1:100,000 sheet, southeastern Iran. Iran J Earth Sci 6:1–11

Moon WM (1990) Integration of geophysical and geological data using evidential belief function. IEEE Trans Geosci Remote Sens 28:711–720

Moradi M, Basiri S, Kananian A, Kabiri K (2015) Fuzzy logic modeling for hydrothermal gold mineralization mapping using geochemical, geological, ASTER imageries and other geo-data, a case study in Central Alborz, Iran. Earth Sci Inf 8:197–205

Moradian A (1997) Geochemistry, geochronology and petrography of feldspathoid bearing rocks in Urumieh-Dokhtar volcanic belt, Iran. Unpublished PhD thesis, University of Wollongong, Australia: 412 pp

Nabighian MN (1972) The analytic signal of two-dimensional magnetic bodies with polygonal cross-section: its properties and use for automated anomaly interpretation. Geophysics 37:507–517

Nabighian MN (1974) Additional comments on the analytic signal of two dimensional magnetic bodies with polygonal cross-section. Geophysics 39:85–92

Nabighian MN (1984) Toward a three-dimensional automatic interpretation of potential field data via generalized Hilbert transforms: fundamental relations. Geophysics 49:780–786

Nykänen V (2008) Radial basis function link nets used as a prospectivity mapping tool for orogenic gold deposits within the Central Lapland Greenstone Belt, northern Fennoscandian Shield. Nat Resour Res 17:29–48

Nykänen V, Salmirinne H (2007) Prospectivity analysis of gold using regional geophysical and geochemical data from the Central Lapland Greenstone Belt, Finland. Geological Survey of Finland pp. 251–269

Omrani J, Agard P, Whitechurch H, Benoit M, Prouteau G, Jolivet L (2008) Arc-magmatism and subduction history beneath the Zagros Mountains, Iran: a new report of adakites and geodynamic consequences. Lithos 106:380–398

Opricovic S (1998) Multicriteria optimization of civil engineering systems. Faculty of Civil Engineering, Belgrade

Opricovic S, Tzeng GH (2004) Compromise solution by MCDM methods: a comparative analysis of VIKOR and TOPSIS. Eur J Oper Res 156:445–455

Paasche H, Eberle DG (2009) Rapid integration of large airborne geophysical data suites using a fuzzy partitioning cluster algorithm: a tool for geological mapping and mineral exploration targeting. Explor Geophys 40:277–287

Pan GC, Harris DP (2000) Information synthesis for mineral exploration. Oxford University Press, New York, 461 pp

Parsa M, Maghsoudi A, Yousefi M, Sadeghi M (2016a) Prospectivity modeling of porphyry-Cu deposits by identification and integration of efficient mono-elemental geochemical signatures. J Afr Earth Sci 114:228–241

Parsa M, Maghsoudi A, Yousefi M, Sadeghi M (2016b) Recognition of significant multi-element geochemical signatures of porphyry Cu deposits in Noghdouz area, NW Iran. J Geochem Explor 165:111–124

Pazand K, Hezarkhani A (2015) Porphyry Cu potential area selection using the combine AHP - TOPSIS methods: a case study in Siahrud area (NW, Iran). Earth Sci Inf 8:207–220

Pazand K, Hezarkhani A, Ataei M (2012) Using TOPSIS approaches for predictive porphyry Cu potential mapping: a case study in Ahar-Arasbaran (NW-Iran). Comput Geosci 49:62–71

Porwal A, Carranza EJM, Hale M (2003) Artificial neural networks for mineralpotential mapping: a case study from Aravalli Province, Western India. Nat Resour Res 12:156–171

Porwal A, Carranza EJM, Hale M (2004) A hybrid neuro-fuzzy model for mineral potential mapping. Math Geol 36:803–826

Porwal A, Carranza EJM, Hale M (2006) Bayesian network classifiers for mineral potential mapping. Comput Geosci 32:1–16

Ranjbar H, Honarmand M (2004) Integration and analysis of airborne geophysical and ETM+ data for exploration of porphyry type deposits in the Central Iranian Volcanic Belt using fuzzy classification. Int J Remote Sens 25:4729–4741

Ranjbar H, Masoumi F, Carranza EJM (2011) Evaluation of geophysics and spaceborne multispectral data for alteration mapping in the Sar Cheshmeh mining area, Iran. Int J Remote Sens 32:3309–3327

Rodriguez-Galiano VF, Chica-Olmo M, Chica-Rivas M (2014) Predictive modelling of gold potential with the integration of multi-source information based on random forest: a case study on the Rodalquilar area, Southern Spain. Int J Geogr Inf Sci 28:1336–1354

Sadeghi B, Khalajmasoumi M (2015) A futuristic review for evaluation of geothermal potentials using fuzzy logic and binary index overlay in GIS environment. Renew Sust Energ Rev 43:818–831

Sadeghi B, Khalajmasoumi M, Afzal P, Moarefvand P (2014) Discrimination of iron high potential zones at the Zaghia iron ore deposit, Bafq, using index overlay GIS method. Iran J Earth Sci 6: 91–98

Siemon B (2001) Improved and new resistivity-depth profiles for helicopter electromagnetic data. J Appl Geophys 46:65–76

van der Meer FD, van der Werff HMA, van Ruitenbeek FJA, Hecker CA, Bakker WH, Noomen MF, van der Meijde M, Carranza EJM (2012) Multi and hyperspectral geological remote sensing: a review. Int J Appl Earth Obs Geoinf 14:112–128

Yousefi M, Carranza EJM (2015a) Geometric average of spatial evidence data layers: a GIS-based multi-criteria decision-making approach to mineral prospectivity mapping. Comput Geosci 83:72–79

Yousefi M, Carranza EJM (2015b) Fuzzification of continuous-value spatial evidence for mineral prospectivity mapping. Comput Geosci 74:97–109

Yousefi M, Carranza EJM (2015c) Prediction-area (P-A) plot and C-A fractal analysis to classify and evaluate evidential maps for mineral prospectivity modeling. Comput Geosci 79:69–81

Yousefi M, Carranza EJM (2016) Data-driven index overlay and Boolean logic mineral prospectivity modeling in Greenfields exploration. Nat Resour Res 25:3–18

Yousefi M, Nykänen V (2016) Data-driven logistic-based weighting of geochemical and geological evidence layers in mineral prospectivity mapping. J Geochem Explor 164:94–106

Zuo R, Carranza EJM (2011) Support vector machine: a tool for mapping mineral prospectivity. Comput Geosci 37:1967–1975